NIH Public Access
Author Manuscript
Nat Methods. Author manuscript; available in PMC 2012 July 10.

Published in final edited form as:
Nat Methods. ; 9(3): 273–276. doi:10.1038/nmeth.1857.

An artery-specific fluorescent dye for studying neurovascular coupling

Zhiming Shen[1,2], **Zhongyang Lu**[1,2], **Pratik Y Chhatbar**[1], **Philip O'Herron**[1], and **Prakash Kara**[1]

[1]Department of Neurosciences, Medical University of South Carolina, Charleston, South Carolina, USA

Abstract

We demonstrate that Alexa Fluor 633 hydrazide (Alexa Fluor 633) selectively labels neocortical arteries and arterioles by binding to elastin fibers. We measured sensory stimulus–evoked arteriole dilation dynamics in mouse, rat and cat visual cortex using Alexa Fluor 633 together with neuronal activity using calcium indicators or blood flow using fluorescein dextran. Arteriole dilation decreased fluorescence recorded from immediately underlying neurons, representing a potential artifact during neuronal functional imaging experiments.

Energy demands of electrically active neurons in the brain are met by regulating blood flow[1]. Active neurons and astrocytes release neurotransmitters that regulate the diameter of blood vessels, which in turn changes blood flow[1–3]. However, the spatial precision of these 'neurovascular coupling' events *in vivo* is largely unknown. For example, a single functional magnetic resonance imaging (MRI) voxel of 1 mm^3 in the cerebral cortex contains ~100,000 neurons[4]. One cubic millimeter of the visual cortex contains precise neuronal maps for all stimulus orientations[5], directions[6] and depths[7] for a given point in visual space. Yet the extent to which blood vessels are locally 'tuned' within and across different categories of sensory stimuli is unknown. Thus, the efficiency of neurovascular coupling in the neocortex remains unclear and so is the interpretation of the underlying source of functional MRI signals[8]. Studies of neurovascular coupling would benefit from the development of dyes that specifically label the different components of the vasculature *in vivo*. Here we report an artery-specific dye, Alexa Fluor 633, and show that it enhances existing methods for studying vessel dynamics and neural activity in the mammalian neocortex.

We originally used long-wavelength Alexa dyes[9] to intracellularly label individual neurons in the rodent and cat neocortex and reconstruct their dendrites in three dimensions. When

Correspondence should be addressed to P.K. (kara@musc.edu).
[2]These authors contributed equally to this work.

Note: Supplementary information is available on the Nature Methods website.

AUTHOR CONTRIBUTIONS

P.K. conceived and designed the study, except the head angle with dip artifact experiments (Z.S.). All authors performed *in vivo* vessel imaging experiments. Z.S. did *in vivo* calcium imaging and head-angle experiments. Z.L. did histology on brain and femoral vessel tissue samples. P.K. did histology of mouse aorta, mouse kidney and human aorta tissues. P.K., Z.S., P.Y.C. and P.O. analyzed the *in vivo* vessel dilation and velocity data. P.K. and Z.S. analyzed the *in vivo* calcium imaging and single-cell electroporation data. All authors discussed results. P.K. wrote the manuscript.

COMPETING FINANCIAL INTERESTS

The authors declare competing financial interests: details accompany the full-text HTML version of the paper at http://www.nature.com/naturemethods/.

Reprints and permissions information is available online at http://www.nature.com/reprints/index.html.

NIH-PA Author Manuscript
NIH-PA Author Manuscript
NIH-PA Author Manuscript

NIH-PA Author Manuscript

NIH-PA Author Manuscript

NIH-PA Author Manuscript

performing these experiments, under continuous guidance of two-photon microscopy, we found that single brief (1 s) puffs of Alexa Fluor 633 from a patch pipette into the extracellular space of the cerebral cortex resulted in instantaneous ultrabright labeling of a subset of vessels in the immediate vicinity of the injection site (Fig. 1a). The two-photon laser powers we used for imaging Alexa Fluor 633 did not lead to any autofluorescence signal from the tissue (Fig. 1b). Progressively larger puffs of Alexa Fluor 633 labeled more vessel surface area (Fig. 1c). But some adjacent and overlapping blood vessels, visible after intravenous injection of fluorescein dextran (Fig. 1d), were not labeled by Alexa Fluor 633. Examining hue differences in bright-field images of vessels on the cortical surface and/or observing the time delay between the filling of arteries and veins after intravenous injection of fluorescein dextran, we determined that Alexa Fluor 633–labeled arteries but not veins in mouse, rat and cat neocortex (Supplementary Figs. 1–3 and Supplementary Video 1).

To determine feasibility of using Alexa Fluor 633 to label vessels in intact dura or thin skull[10] preparations, we applied Alexa Fluor 633 via intravenous injection (in mice, rats and cats; Online Methods). As expected, the dye was initially visible in the lumen of all blood vessels. But within 30–90 min, the kidneys appeared to filter much of the luminal Alexa Fluor 633 and bright labeling of arteriole walls remained (Fig. 1e,f). Bright arteriole-wall labeling persisted for more than 24 h after injection (Supplementary Fig. 4).

Whether we applied Alexa Fluor 633 *in vivo* (intravenously or by local micropipette injection) or on the surface of histological sections (topically), microvessels (≤10 μm diameter), venules and veins were not labeled in mice, rats and cats (Fig. 1g, Supplementary Figs. 1–10 and Supplementary Videos 2 and 3). All ≥15-μm-diameter arterioles were labeled, but no ≤ 10-μm-diameter arterioles were labeled (Supplementary Figs. 6–10). This diameter-dependent Alexa Fluor 633 labeling occurred regardless of whether the unlabeled branches were surface arterioles or offshoots from penetrating arterioles (Supplementary Figs. 6–8). Thus, rather than a progressive decrease in Alexa Fluor 633 labeling along the length of a vessel, there was a binary switch to no labeling after a branch point if the daughter branch was small enough (Supplementary Figs. 6–8).

To physiologically cross-validate that only arteries and arterioles were labeled by Alexa Fluor 633, we analyzed vessel dynamics in response to sensory stimulation. We injected mice, rats and cats with Alexa Fluor 633 and fluorescein dextran, and imaged neocortical arterioles and venules with two-photon microscopy while presenting drifting square-wave grating visual stimuli. We examined vessels with diameters of 17–114 μm and quantitatively determined the time course of sensory stimulus–evoked vessel dilation (Fig. 1h). Only vessel walls labeled with Alexa Fluor 633 showed stimulus-evoked dilations (10 mouse, 15 rat and 10 cat arteriole branches in (two mice, five rats and six cats); for example, Supplementary Video 4). The dilation dynamics were consistent with those observed in arterioles: relatively short latency and large amplitude[11,12]. Upon visual stimulation we observed an absolute increase in arteriole diameter ranging from ~1 μm for arterioles with a baseline diameter of 20 μm, to ~11 μm for arterioles with a baseline diameter of 114 μm. The average percentage change in dilation of Alexa Fluor 633–labeled arterioles was indistinguishable among the three species examined: analysis of variance (ANOVA) $P = 0.24$, Lilliefors $P > 0.20$, mean ± s.e.m. for mouse, 6.8 ± 0.7% ($n = 10$ arteriole branches); rat, 8.9 ± 0.8% ($n = 15$ branches); and cat, 7.5 ± 0.9% ($n = 15$ branches). When we recorded venule responses simultaneously with arteriole responses, venules never showed significant diameter changes in response to visual stimuli by any of the following criteria: ANOVA test was $P > 0.05$ across blank and n test visual stimuli, the percentage change of visually evoked dilation was < 1%, and visually evoked dilations did not exceed 3 s.d. above the mean pre-stimulation baseline diameter ($n = 4$ vein branches in two mice and $n = 9$ vein branches in two rats) (Supplementary Fig. 11). Many within and across controls in cats showed that

NIH-PA Author Manuscript

NIH-PA Author Manuscript

NIH-PA Author Manuscript

local pipette and intravenous application of Alexa Fluor 633 did not alter individual neuronal responsiveness and selectivity to sensory visual stimuli (Supplementary Figs. 12 and 13). The cat's heart rate and electroencephalography activity were also unaffected by application of Alexa Fluor 633 (Supplementary Fig. 14).

To test for arteriole specificity of Alexa Fluor 633 among the general class of Alexa Fluor hydrazide dyes, we compared the *in vivo* efficacy of three red Alexa dye variants (Alexa Fluors 594, 633 and 647) in the rat neocortex. Alexa Fluor 594 was the most similar enantiomer-like variant to Alexa Fluor 633 (Fig. 1i). Alexa Fluor 633 produced the highest relative brightness of arteriole wall labeling (Online Methods) across different experiments (Fig. 1j; ANOVA $P < 0.0001$; unequal N honestly significant difference (HSD) = 0.0001 for Alexa Fluor 633 versus 594 and Alexa Fluor 633 versus 647). Arteriole wall binding for Alexa Fluors 594 and 647 was indistinguishable (unequal N HSD = 0.1).

Having determined the *in vivo* selectivity of Alexa Fluor 633 for labeling arteries, we next identified the component of the arteriole wall Alexa Fluor 633 bound by using histological techniques in mouse, rat, macaque monkey and human tissue (Fig. 1k–n and Supplementary Figs. 15–18). Arterioles in the cerebral cortex have five characteristic layers, but only one layer appeared to be labeled by Alexa Fluor 633 in mice, rats and monkeys (Fig. 1k–l and Supplementary Figs. 9, 10 and 15a–c). We performed immunohistochemistry for smooth muscle (antibody to alpha smooth muscle actin (α-SMA)) or endothelial cells (antibody to glucose transporter 1 (GLUT1)) together with Alexa Fluor 633 dye application. Alexa Fluor 633 labeling overlapped with neither α-SMA labeling (Fig. 1k; $n = 2$ macaque monkeys, 4 mice and 3 rats; Pearson's correlation coefficient $R_r < 0$) nor endothelial cells (Fig. 1l; $n = 4$ mice and 3 rats; Pearson's correlation coefficient $R_r < 0$). Pericytes were not labeled by Alexa Fluor 633 (Supplementary Fig. 9).

Not present in cerebral venules and capillaries, but highly characteristic of cerebral arterioles, is a layer of elastic lamina that lies between the smooth muscle and the endothelial cell layers (Supplementary Fig. 15a). Antibodies to elastin are unreliable for distinguishing among adjacent arteriole wall layers (unpublished observations; D. Li, P.K. and Z.L.) and may compete with Alexa Fluor 633 on elastin fiber binding sites. Therefore to test whether Alexa Fluor 633 specifically labeled elastin fibers on artery walls, we used two strategies. First, we examined other organs in which it is well established that two or six layers of elastin are present on the artery: mouse femoral artery has two characteristic elastin layers and mouse aorta has six. Indeed Alexa Fluor 633 selectively labeled two and six layers on femoral artery and aorta, respectively (Fig. 1m and Supplementary Fig. 15d–f). Femoral arteries had a thin endothelial basement membrane adjacent and nonoverlapping with Alexa Fluor 633 staining (Fig. 1n; Pearson's $R_r < 0$), suggesting that Alexa Fluor 633 was not binding to the endothelial basement membrane. Second, we considered previously published work[13], which showed that using very high power two-photon laser excitation, elastin fibers in artery walls are autofluorescent in the blue-green spectral emission range. High laser powers are incompatible with physiology (owing to phototoxicity) and produce near instantaneous bleaching of Alexa Fluor 633 (Supplementary Fig. 15e). However, in mouse brain and aorta tissue sections labeled with Alexa Fluor 633, we performed sequential two-photon imaging on the same sample by first using low laser power (2–3 mW) to image Alexa Fluor 633 (red emission) and then using high laser power (20–30 mW) to image blue-green autofluorescence (Supplementary Fig. 16). In both brain and aorta tissue samples, Alexa Fluor 633 labeling and endogenous blue-green autofluorescence overlapped greatly (Pearson's $R_r > 0.8$; $n = 2$ mice). Our histology and *in vivo* data confirmed that Alexa Fluor 633 selectively bound elastin fibers on artery and arteriole walls.

NIH-PA Author Manuscript

NIH-PA Author Manuscript

NIH-PA Author Manuscript

Alexa Fluor 633 artery wall labeling and sensory-evoked dilation measurements were compatible with the imaging of neuronal activity and blood-velocity measurements. We tracked neural activity in the cat primary visual cortex using two-photon imaging of the calcium indicator Oregon Green Bapta-1 and simultaneously monitored sensory-evoked responses in arterioles using Alexa Fluor 633 (Fig. 2a–d). In rats, we also measured blood velocity in vessels using the lumen-labeling dye fluorescein dextran (Fig. 2e–g). Additionally, in the early phase after intravenous injection of Alexa Fluor 633, that is, before it is cleared from the plasma, Alexa Fluor 633 itself can be used to measure blood velocity (Supplementary Fig. 19). To test the use of Alexa Fluor 633 for mapping the sensory-stimulus selectivity of individual arterioles, we presented cats with drifting grating visual stimuli in nine different positions and quantified the dilation in individual arterioles (Fig. 2h,i).

We discovered that arteriole dilation decreased the fluorescence recorded from immediately underlying neurons, producing an imaging artifact that has, to our knowledge, not been reported and/or factored into quantifying calcium signals from neurons: we labeled single neurons in layer 2/3 of visual cortex by single-cell electroporation of Alexa Fluor 594 (31 neurons in 4 rats, 1 cat and 1 mouse). We specifically targeted neurons that were located directly below surface blood vessels with diameters of 20–80 μm (Fig. 3). When these vessels were arterioles (for example, Fig. 3a,b), visual stimuli evoked 5–20% dips in fluorescence from neurons ($n = 19$ neurons; $P < 0.005$ two-tailed t-test; Lilliefors $P > 0.2$). Neurons labeled below veins (for example, Fig. 3c,d) showed no dips in fluorescence upon the presentation of visual stimuli ($n = 12$ neurons; $P > 0.05$ two-tailed t-test; Lilliefors $P > 0.2$).

To determine whether the two-photon laser beam interacting with the dilating arteriole was producing the dip in fluorescence, we imaged a given cortical neuron in two ways. First we imaged in mice and rats the cortical neuron through a surface arteriole (as above), producing a dip in its fluorescence. Then we rotated the animal's head up to 50° so that the two-photon beam impacted directly on the neuron's cell body (Fig. 3e–i). In this situation, the dip in neuronal fluorescence was reduced or eliminated altogether (for example, Fig. 3i; $n = 8$ neurons; $P = 0.01$ paired t-test for dependent samples). Arterioles always dilated in response to the visual stimuli irrespective of the head angle. We intentionally performed these 'dip artifact' experiments with a nonfunctional dye (Alexa Fluor 594) rather than using calcium indicators so as to capture the pure artifact without contamination from functional neural signals (but see Supplementary Note 1).

Here we demonstrated that Alexa Fluor 633 selectively bound elastin fibers in arterial walls in mouse, rat, cat and macaque monkey brains. Alexa Fluor 633 did not label veins, capillaries, neurons, astrocytes or pericytes. Other structurally similar dyes (Alexa Fluors 594 and 647) bound arterial walls less effectively. We showed Alexa Fluor 633 is nontoxic, can be used in combination with various green dyes and to monitor changes in arterial dynamics in response to sensory stimulation. Considering the large number of research studies now using two-photon calcium indicator imaging from neurons, our *in vivo* arteriole wall labeling method can be used to identify, exclude and correct changes in neuronal fluorescence that are due to arteriole dilation. These assessments extend the use of Alexa Fluor 633 well beyond its previously reported use in isolated and dissected arteries[14,15]. This is, to our knowledge, the first reported compound with selectivity for brain arterioles *in vivo* (see Supplementary Note 2 for discussion on selectivity of Alexa Fluor 633 and other rhodamine derivatives).

Alexa Fluor 633 has great potential to be used for the study of arteriole dilation dynamics in various mammalian species and is a new and simple tool for neurovascular coupling

NIH-PA Author Manuscript

NIH-PA Author Manuscript

NIH-PA Author Manuscript

research. Alexa Fluor 633 can be used to label arteriole walls locally using micropipette injection or globally using intravenous administration. In the future, Alexa Fluor 633–like dyes may serve as the basis for the design of therapeutic compounds that bind to arteriole walls but do not enter the parenchyma when injected intravenously as well as for the development of MRI and positron emission tomography analogs for noninvasive imaging in humans.

ONLINE METHODS

Animals and human tissue samples

Five mammalian species were used in this study. The Institutional Animal Care and Use Committee of the Medical University of South Carolina approved all animal experiments. Wild-type C57BL/6 mice (15 males, post-natal days 35–60) and Long Evans rats (24 males, postnatal days 29–48) and cats (13 of either sex, postnatal day 28 to > 2.5 kg adult) were used for *in vivo* physiology and postmortem histology studies. Mice and rats were purchased from Charles River and Harlan Laboratories. Cats were purchased from Liberty Research. The mice, rats and cats were housed in independent facilities specifically designed for each species. Mice were housed in ventilated racks. Rats were housed in microisolator cages. Cats were housed in open condo-style cages with food bowls, water bottles and litter boxes and had unrestricted access to roam in the confines of the room in which they were located. All animal facilities maintained >15 air changes per hour with centrally controlled and monitored humidity and 12 h day–12 h night lighting cycles. All animals received environmental species-specific enrichment. Macaque monkey postmortem samples obtained directly from the University of California at San Francisco (two samples) and human postmortem aorta or coronary artery samples from ILSbio (two samples) were used for histochemistry and immunofluorescence only. Because the human tissue samples were postmortem, deidentified and not collected for the specific purpose of this study, our Institutional Review Board for Human Research Experiments determined that our dye labeling of human tissue was not ‘Human Subject Research’; no Institutional Review Board exemption was required.

In vivo two-photon imaging in mice, rats and cats

Mice were anesthetized with urethane (1.5 g kg^{-1} intraperitoneally), supplemented with ketamine (10–30 mg kg^{-1}) and xylazine (1–3 mg kg^{-1}) during surgery. In rats, anesthesia was induced with a fentanyl cocktail (0.04–0.06 mg kg^{-1} fentanyl citrate, 3.75–6.25 mg kg^{-1} midazolam and 0.19–0.31 mg kg^{-1} dexmedetomidine, all administered intraperitoneally). During two-photon imaging, the doses were lowered (0.02–0.03 mg kg^{-1} h^{-1} fentanyl citrate, 1.50–2.50 mg kg^{-1} h^{-1} midazolam and 0.15–0.25 mg kg^{-1} h^{-1} dexmedetomidine) and administered via continuous intra-peritoneal infusion using a catheter connected to a syringe pump. In cats, anesthesia was induced with an intramuscular injection of ketamine (10–20 mg kg^{-1}) and acepromazine (0.2 mg kg^{-1}), continued with isoflurane (1–2% in surgery and 0.5–1.0% during imaging). Cats were paralyzed with vecuronium bromide (0.2 mg kg^{-1} h^{-1}, intravenously), and expired CO_2 was regulated at 3.5–4.5% via mechanical ventilation. In each of the three species, a customized titanium or stainless steel headplate was attached to the skull using dental cement. Then a craniotomy was performed over the primary visual cortex, the dura was reflected, and the underlying cortex was covered with agarose. Removal of the dura was necessary in cats and rats but was left intact in mice. Individual Alexa dyes were injected into the visual cortex by a 2-μm-diameter micropipette (50 μM dye concentration) or administered via intravenous injection (1–2 mg kg^{-1}; tail vein in rodents and femoral vein in cats). Thick dura made topical application of Alexa dyes ineffective. Provided that excessive laser power was not used, a single injection of Alexa Fluor 633 (Alexa 633) resulted in brightly labeled arteriole walls for the entire *in*

NIH-PA Author Manuscript

NIH-PA Author Manuscript

NIH-PA Author Manuscript

vivo recording period, at least 26 h in our acute experiments (Supplementary Fig. 4). The cell-permeant calcium indicator Oregon Green 488 Bapta-1 AM (Invitrogen) was injected into layer 2/3 visual cortex as previously described[7]. Fluorescence from neurons and vessels was monitored with a customized Prairie Technologies microscope and light path (Supplementary Fig. 20) that was optimized for *in vivo* experiments in mouse, rat and cat preparations, and coupled with a Mai Tai XF (Newport Spectra-Physics) mode-locked Ti:sapphire laser (810 nm). Excitation light was focused by a high-numerical-aperture (1.0 NA) water-immersion objective (Olympus XLUMPLFLN 20×) and beam expansion optics was used to overfill the back aperture (Supplementary Fig. 20). For deep *in vivo* imaging up to 550 μm below the cortical surface (for example, Supplementary Fig. 7), we used a 1.1 NA water-immersion objective (Nikon CFI Apo LWD 25×). Two non-descanned photo-multiplier tube (PMT) detector channels (Hamamatsu) were used with barrier filters (Chroma). Barrier filters were customized as needed to match particular fluorophores of interest: ET 525/50m-2p for Oregon Green 488 Bapta-1 AM and fluorescein dextran 70 kDa and 2,000 kDa (Sigma-Aldrich); ET 665/40m-2p for Alexa Fluors 633 and 647 hydrazide (Invitrogen), HQ 645/70m-2p for Alexa Fluor 594 hydrazide (Invitrogen) and BG22 for blue-green autofluorescence. In addition to barrier filter and PMT dichroic selection, detection of long-wavelength dyes such as Alexa Fluors 633 and 647 hydrazide also required careful selection of the primary dichroic (700dcxr, Chroma) and blocking filter (ET 700sp-2p8; Chroma).

In vivo imaging of the arterial and venous filling phases in cerebral cortex

Using a 4× air objective (Olympus UPLFLN, NA 0.13), time-lapse video of the arterial and venous filling phases upon intravenous administration of fluorescein dextran (~50 mg kg^{-1} via a 5% stock solution, injecting 0.1 ml per 100 g of body weight) was recorded from the cat visual cortex with an Adimec 1000 monochrome charge-coupled device (CCD) camera (50 Hz frame rate, 498 × 498 pixels; see Supplementary Figure 1 and Supplementary Video 1). The Adimec 1000 was attached directly to the c-mount camera port of the Prairie Technologies microscope. An Exfo X-CITE 120Q light source was used in combination with a FITC epi-fluorescence filter set (Chroma) placed before the CCD camera to collect fluorescein dextran fluorescence.

Visual stimulation

Mice, rats and cats viewed drifting square wave grating stimuli (1.5–2 Hz, 100% contrast) presented on a computer display monitor while we performed two-photon imaging at a particular site in the primary visual cortex. In experiments that required the assessment of vessel dilation and/or red blood cell velocity to sensory stimulation, visual stimuli were presented for 4–8 s interspersed by a two- to fivefold longer period of blank (equiluminant gray screen). The duration of the stimulation period, for example, 8 s, and the duration of the blank display period, for example, 24 s, was always identical across all 16 or more repeats of a particular two-photon imaging session. For control experiments that required calcium imaging from neurons without an assessment of vessel dilation or red blood cell velocity (for example, Supplementary Figs. 12 and 13), blank display periods were of equal duration to visual stimulation periods[7]. This is because unlike arteriole dilation, neural calcium transients returned to baseline nearly immediately upon extinguishing the visual stimulus[7] (Fig. 2b,c).

In vivo data-analysis overview

All two-photon images of vessels and neurons collected during *in vivo* physiology experiments were analyzed using customized Matlab (MathWorks) software. Some statistical functions not available in Matlab were implemented in Statistica (Statsoft). Three-dimensional rendering and masking of cells and vessels in imaged volumes were performed

NIH-PA Author Manuscript

NIH-PA Author Manuscript

NIH-PA Author Manuscript

using Imaris (Bitplane) (for example, Fig. 3e). Typically a square region of cortex was imaged at 128 × 128 pixels (200 μm per side) to 512 × 512 pixels (600 μm per side) at 0.16–1.64 s per frame. For blood-velocity measurements, line-scan parameters were optimized for a given caliber vessel (2–6 μs pixel^{-1}, 0.23–0.93 μm pixel^{-1} and 0.63–1.7 ms line^{-1}). Movements of the brain from respiratory and heartbeat pulsations were negligible with our established imaging and surgical methods, which sometimes included a lumbar suspension and pneumothorax in cats[5–7]. However, in our vessel dilation analyses, to compensate for very small drifts in baseline vessel diameter over a long recording session containing many hundreds to thousands of imaging frames, the mean vessel diameter for adjacent baseline frames during each blank period epoch and subsequent adjacent baseline frames during the next blank period epoch were linearly interpolated. For calcium imaging from neurons, images were realigned by maximizing the correlation between frames[6]. As brain movement was minimal, realignment did not influence the statistical outcome of responsiveness and tuning-width measurements.

Quantifying vessel dilation and blood velocity *in vivo*

To determine the change in vessel diameter upon sensory stimulation when artery walls were labeled with Alexa 633, we first used a Gaussian filter ($\sigma \approx 1$ μm) to smooth each imaging frame of the time series. Vessel cross-sections were then selected manually using a graphical user interface. When vessels were imaged longitudinally (Fig. 1a,c,e), the cross-section was drawn perpendicular to the two parallel lines that represented each side of the vessel wall. When a vessel was imaged transversely (Fig. 2a), cross-section line segments passed through the center of the circular vessel. Because Alexa 633 labeled the arterioles brightly with minimal dye in the lumen of the vessel and the brain parenchyma (Fig. 1), the profile of image brightness along the cross-section line segment always had only two maxima. Each maximum corresponded to each side of the vessel. The distance between the two maxima of each cross-section line segment represented the diameter of the vessel. The above procedures were used to calculate the diameter in each imaging frame of the time series, resulting in a time course of vessel dilation for each cross-section examined (for example, Figs. 1h and 2d,g,h). The Lilliefors test for normality was satisfied for all vessels examined. Vessels selectively tuned for particular receptive field location was defined by ANOVA across n stimulus periods ($P < 0.05$). Typically, our two-photon imaging frame rates for vessel imaging were slow (1–1.64 s frame^{-1}) but well within the range used in our previous calcium imaging work[5–7]. With faster imaging frame rates (0.16–0.2 s frame^{-1}) we could extract the latency of arteriole dilation relative to the onset of the grating visual stimulus. To determine the latency of dilation upon sensory stimulation, each of n baseline and m stimulus frames were averaged across all repeats. We then performed a linear regression on the rising phase of the vessel dilation response using data points between 20% and 80% to the peak dilation[11] (for example, Fig. 1h). Visually evoked latencies of dilation for arterioles ranged from 0.67 s to 0.99 s ($n = 3$ arteriole branches in two mice and 5 arteriole branches in two rats). To quantify the change in vessel diameter upon sensory stimulation when the lumen of veins and arteries were labeled with fluorescein dextran, we applied the same Gaussian smoothing as described above for Alexa 633–labeled walls. However, maxima with fluorescein dextran labeling did not necessarily correspond with the vessel diameter because the lumen could have near equal brightness at more than two points along the cross-section line segment. Thus, for fluorescein dextran labeling, we calculated the first derivative of the profile of image brightness along the cross-section line segment. The first derivative had a maximum at the wall-lumen interface. Red blood cell velocity was determined from line scans of fluorescein dextran– (or Alexa 633–) labeled lumen of the blood vessel of interest (Supplementary Fig. 19). We used the Radon transform to calculate velocity (in millimeters per second) as described previously[16]. Typically, we calculated the average velocity per block of 300 sequential line scans with an overlap of 100 lines between

NIH-PA Author Manuscript

NIH-PA Author Manuscript

NIH-PA Author Manuscript

blocks. The algorithm was implemented using the Matlab function 'radon'. The time courses of visual stimulus evoked velocity responses (blank versus stimulation periods; for example, Fig. 2f) were smoothed by a 10-point sliding mean.

Quantifying the efficacy of three red Alexa dye variants *in vivo* (Alexa 594, 633 and 647)

We adopted the following standardized protocol in five rats: for each rat, two dyes were compared simultaneously in two adjacent craniotomies or injection sites. Each dye (50 μM solution) was applied locally in the cortex with a 2-μm-diameter tip patch pipette. The patch pipette was positioned ~50 μm below the pial surface and ~50 μm from a wall of the artery of interest. We always applied three pulses to puff out dye from the pipette tip (4 p.s.i. per pulse, 1 s pulse duration). After all unbound dye washed away, we collected two-photon images of longitudinal sections of the vessel walls using very low, 2–3 mW laser power (for example, Fig. 1a). We drew cross-section line segments perpendicular to the two parallel lines that represented each side of the vessel wall, as was done for vessel diameter calculations (see above). The binding efficacy of a given dye *in vivo* was determined as the brightness of the vessel wall versus brightness outside of the vessel wall along individual cross-section line segments. Tukey's HSD post-ANOVA comparisons were used to determine whether the aggregate mean differences in labeling brightness among the Alexa 594, 633 and 647 groups were significantly different (Fig. 1j).

Quantifying neuronal calcium transients

The time course of calcium transients from neurons was used to determine statistically significant visually evoked responses and selectivity using established procedures[5–7]. Briefly, neurons were identified through a series of morphological filters that defined the contours of cell bodies based on intensity, size and shape. Time courses of individual cells were extracted by calculating mean pixel values within cell contours. Visually responsive cells were defined by ANOVA across blank and n test visual stimuli ($P < 0.05$). Cells selective for particular stimuli were defined by ANOVA across n stimulus periods ($P < 0.05$).

Perfusion and histology

A mixture of pentobarbital and phenytoin sodium (Euthasol, 180 mg kg^{-1}, Virbac) was given intraperitoneally to deeply anesthetize (EEG flatlined) and kill (heart rate and respiration fell to zero) mice and rats. The mice and rats were then transcardially perfused with saline followed by 4% paraformaldehyde in phosphate buffer using a peristaltic pump. Brain, aorta, kidneys and femoral vessels were then dissected and incubated with 30% sucrose in phosphate buffer. Then the tissues were placed on dry ice and embedded into optimal cutting temperature (OCT) compound (Tissue-Tek). Tissue sections (40 μm thick) were cut on a vibratome. As we had to perform immunohistochemistry on multiple adjacent components of the vessel wall, it was necessary to ensure that paraformaldehyde fixation itself did not influence antibody binding to vessel lamina. Therefore in a few mice and rats, we performed histology without paraformaldehyde perfusion. In these instances, tissues were dissected immediately after killing, placed on dry ice, embedded in OCT compound and stored at −80 °C. OCT-embedded frozen tissue was cryosectioned (8–10-μm-thick sections). Postmortem blocks of macaque monkey cerebral cortex were also cut on a vibratome (5- and 40-μm-thick sections). Human aorta and coronary samples were flash-frozen directly by ILSbio before our study began and before our request for such samples from them. ILSbio obtained these tissues from healthy subjects with a postmortem interval of ~2 h or less. Human tissue samples were cut in 5-μm-thick sections. During our study, no local or national human tissue bank had cerebral cortex tissue sections from healthy subjects with short postmortem intervals. Short postmortem interval samples from healthy human tissue samples appeared to be necessary for robust labeling of artery and arteriole walls by

NIH-PA Author Manuscript

NIH-PA Author Manuscript

NIH-PA Author Manuscript

Alexa 633 because our anecdotal observations from postmortem tissue samples that had undocumented postmortem intervals, stored in fixative for years and/or associated with extensive neurodegenerative pathology did not yield bright artery- or arteriole-specific labeling with Alexa 633. Our rat and mouse tissues essentially had zero postmortem intervals to transcardial paraformaldehyde perfusion or OCT embedding and flash-freezing. Furthermore, rodent samples were not stored in paraformaldehyde or other fixative for months. We observed no difference in the quality of Alexa 633 binding to artery and arteriole walls using our two methods of histological preparation of rat or mouse tissue. For flash-frozen human tissue, the quality of Alexa 633 labeling of artery walls was equally good irrespective of whether the dye was applied to unfixed or acetone-fixed tissue sections or whether endogenous peroxidase was quenched.

Immunofluorescence analysis, autofluorescence analysis, Alexa 633 labeling and bleaching

Tissue sections were bathed in blocking solution: 3% normal goat serum in phosphate buffered saline (PBS; pH 7.4) for 60 min. The following primary antibodies were applied overnight (one antibody per section, except for triple labeling described below): rabbit antibody to GLUT1 (1:400, Abcam, AB652) as an endothelial cell marker; mouse antibody to actin-α-smooth muscle clone 1A4 (1:400, Sigma-Aldrich, A2547) as a marker for smooth muscle; rabbit antibody to laminin (1:200, Abcam, AB11575) as a maker for endothelial basement membrane, and goat antibody PDGFR-β (1:40, R&D Systems, AF1042) as a marker for pericytes. After three washes for 5 min each in PBS, the following secondary antibodies were applied (one antibody per section, except for triple labeling described below): goat anti-rabbit IgG (FITC) or goat anti-rabbit IgG (Alexa Fluor 488) for GLUT1; goat anti-mouse IgG (FITC) for actin-α-smooth muscle; anti-rabbit IgG (FITC) for laminin and rabbit anti-goat IgG (FITC) for PDGFR-β. The primary antibodies we used were tested for specificity in previous studies[17–20]. But even in our study, the specificity of antibodies used to label smooth muscle, endothelial cells, basement membrane and pericytes was unambiguous via unique morphological features that were labeled (Supplementary Figs. 9, 10 and 15) and negative controls. Using ‘green’ secondary antibodies for smooth muscle, endothelial cells, basement membrane and pericytes enabled us to perform colocalization studies with the ‘red’ arteriole-specific Alexa 633. Consequently, Alexa 633 (1:1,000 dilution from 2 mM stock) was added to the histological tissue sections for 1–2 min and rinsed. The tissue sections on the glass slides were then prepared for confocal, two-photon or epi-fluorescence microscopy by applying Fluoromount aqueous mounting medium (Sigma) and covered by a coverslip. Two-color histological fluorescence images (2,048 × 2,048 pixels) were typically collected on a Leica TCS SP5 confocal laser scanning microscope using a very high NA (1.47) oil-immersion objective (Leica HCX PL APO 63×). Using individual laser lines (Ar 488, He 543 and 633 nm) together with the 1 nm tuning resolution of the prism-based spectral emission filters on the Leica confocal microscope ensured that red and green fluorescence detection bandwidths were completely nonoverlapping for the dyes of interest. To further minimize bleed through, we acquired confocal images exclusively by sequential scanning[21,22]. Some histological sections, particularly those labeled with one exogenous fluorescent label, for example, Alexa 633, were examined using our *in vivo* two-photon microscope. Two-photon excitation of brain and aorta tissue sections was critical for determining whether the signature autofluorescence of elastin fibers[13] (blue-green emission) visible with high two-photon laser power (>20–30 mW, measured at the front aperture of the objective lens) overlapped with Alexa 633 labeling that was evident with low (2 mW) power (Supplementary Fig. 16). For these autofluorescence tests, we used emission filters ET 665/40m-2p for Alexa 633 on one PMT channel and BG22 for blue-green autofluorescence on a second PMT channel. No bleaching of Alexa 633 occurred with low two-photon laser power, but using >20–30 mW to thin

NIH-PA Author Manuscript

NIH-PA Author Manuscript

NIH-PA Author Manuscript

tissue sections on glass slides produced near-instantaneous bleaching (Supplementary Fig. 15e). Because our Leica confocal and Prairie Technologies two-photon imaging systems were each equipped with only two PMTs, triple-labeled tissue sections with Alexa 633, PDGFR-β antibodies and 4′,6-diamidino-2-phenylindole (DAPI) or PDGFR-β antibodies, GLUT1 antibodies and DAPI were examined on a Nikon 90i epi-fluorescence microscope, using a CFI Plan Fluor 40× oil NA 1.3 objective and FITC, Texas Red and DAPI filter sets. PDGFR-β antibody, GLUT1 antibody and DAPI triple labeling (Supplementary Fig. 9b) required the following secondary antibodies: donkey anti-goat IgG (Alexa 594) for PDGFR-β and bovine IgG (FITC) for GLUT1. Quantitative localization[21,22] analysis including Pearson's correlation coefficient after background subtraction[21,22] was performed using CoLocalizer Pro (CoLocalization Research Software).

Supplementary Material

Refer to Web version on PubMed Central for supplementary material.

Acknowledgments

We thank W. Argraves (Medical University of South Carolina) for mouse aorta samples; J. Horton (University of California at San Francisco) for macaque monkey brain tissue; C. Beeson and Y. Peterson for modeling the structural overlap of various Alexa dyes; P. Bell for dissecting mouse kidneys; D. Leopold and A. Silva for discussion on MRI applications; R. Gourdie for discussion of Alexa Fluor 633 binding sites on artery walls; E. Vought for creating illustrations; P. Mulholland for help with using Imaris software; M. Levy and A. Schramm for comments on the manuscript. This work was supported by grants from the US National Eye Institute (R01EY017925 and R21EY020985) and funds from the Medical University of South Carolina to P.K.

References

1. Attwell D, et al. Nature. 2010; 468:232–243. [PubMed: 21068832]
2. Kleinfeld D, et al. Front Neuroenergetics. 2011; 3:1. [PubMed: 21559095]
3. Iadecola C, Nedergaard M. Nat Neurosci. 2007; 10:1369–1376. [PubMed: 17965657]
4. O'Kusky J, Colonnier M. J Comp Neurol. 1982; 210:278–290. [PubMed: 7142443]
5. Ohki K, et al. Nature. 2006; 442:925–928. [PubMed: 16906137]
6. Ohki K, Chung S, Ch'ng YH, Kara P, Reid RC. Nature. 2005; 433:597–603. [PubMed: 15660108]
7. Kara P, Boyd JD. Nature. 2009; 458:627–631. [PubMed: 19158677]
8. Logothetis NK. Nature. 2008; 453:869–878. [PubMed: 18548064]
9. Berlier JE, et al. J Histochem Cytochem. 2003; 51:1699–1712. [PubMed: 14623938]
10. Drew PJ, et al. Nat Methods. 2010; 7:981–984. [PubMed: 20966916]
11. Tian PF, et al. Proc Natl Acad Sci USA. 2010; 107:15246–15251. [PubMed: 20696904]
12. Drew PJ, Shih AY, Kleinfeld D. Proc Natl Acad Sci USA. 2011; 108:8473–8478. [PubMed: 21536897]
13. Zipfel WR, et al. Proc Natl Acad Sci USA. 2003; 100:7075–7080. [PubMed: 12756303]
14. Kansui Y, Garland CJ, Dora KA. Cell Calcium. 2008; 44:135–146. [PubMed: 18191200]
15. Clifford PS, et al. Arterioscler Thromb Vasc Biol. 2011; 31:2889–2896. [PubMed: 21979438]
16. Drew PJ, Blinder P, Cauwenberghs G, Shih AY, Kleinfeld D. J Comput Neurosci. 2010; 29:5–11. [PubMed: 19459038]
17. Carlson TR, et al. Proc Natl Acad Sci USA. 2005; 102:9884–9889. [PubMed: 15994223]
18. Li Y, Lu Z, Keogh CL, Yu SP, Wei L. J Cereb Blood Flow Metab. 2007; 27:1043–1054. [PubMed: 17077815]
19. Svedin P, Hagberg H, Savman K, Zhu C, Mallard C. J Neurosci. 2007; 27:1511–1518. [PubMed: 17301159]
20. Bell RD, et al. Neuron. 2010; 68:409–427. [PubMed: 21040844]
21. Bolte S, Cordelieres FP. J Microsc. 2006; 224:213–232. [PubMed: 17210054]

22. Zinchuk V, Grossenbacher-Zinchuk O. Prog Histochem Cytochem. 2009; 44:125–172. [PubMed: 19822255]

NIH-PA Author Manuscript

NIH-PA Author Manuscript

NIH-PA Author Manuscript

NIH-PA Author Manuscript

NIH-PA Author Manuscript

NIH-PA Author Manuscript

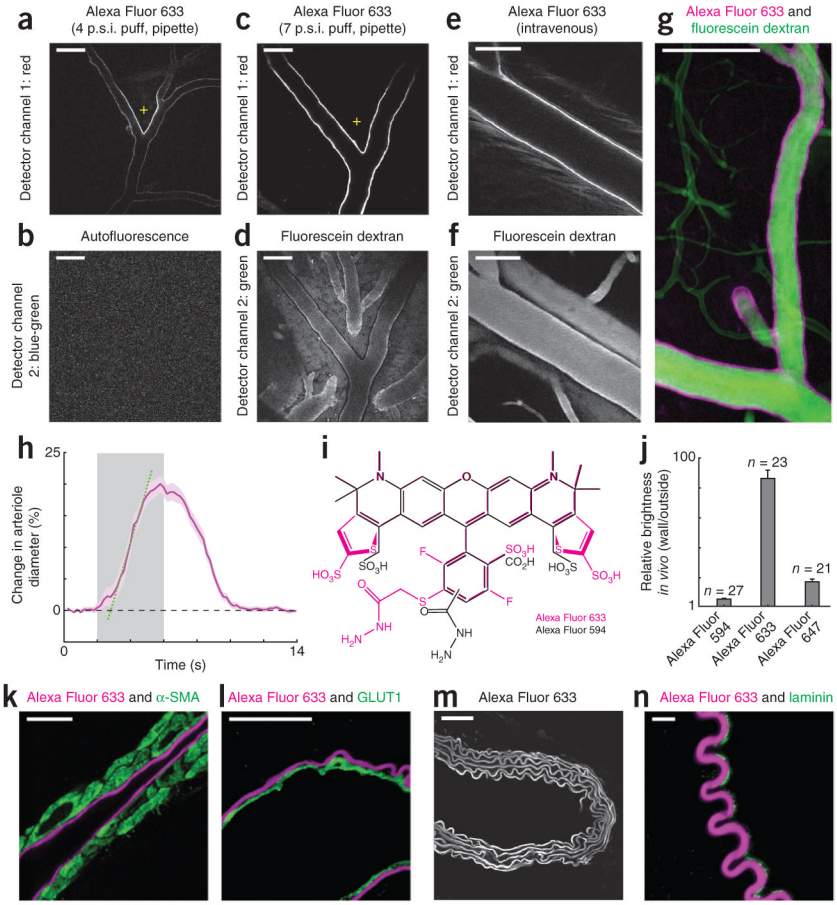

Figure 1.

Selective labeling of artery walls by Alexa Fluor 633. (**a**,**b**) Two-photon microscopy image of the mouse visual cortex after a 4 pounds per square inch (p.s.i.) 1-s puff of Alexa Fluor 633 from a micropipette (**a**; + indicates tip position) and an autofluorescence image (**b**) obtained simultaneously *in vivo* using 2 mW laser power. (**c**,**d**) Image from the rat visual cortex after a 7 p.s.i. 1-s puff of Alexa Fluor 633 *in vivo* (**c**) and fluorescence image of the same cortical site taken after intravenous injection of fluorescein dextran (**d**). (**e**,**f**) Images of arteriole walls in mouse visual cortex after intravenous injection of Alexa Fluor 633 (**e**) and of the same site after injection of fluorescein dextran (**f**). (**g**) Average intensity 66 μm *z*-dimension projection image from mouse visual cortex after an intravenous injection of fluorescein dextran and local pipette injection of Alexa Fluor 633. (**h**) Dilation of an Alexa Fluor 633–labeled arteriole from the rat visual cortex in response to drifting grating visual stimuli (gray bar). The intersection between the regression line (dotted green) and zero level (dashed black) represents the latency of dilation (0.8 s). Purple shading indicates s.e.m. (n = 16 trials). (**i**) Molecular structures of Alexa Fluors 633 and 594. (**j**) Relative brightness of arteriole walls labeled with Alexa Fluors 594, 633 and 647. Data were pooled from five experiments in the rat cortex (error bars, s.e.m.). (**k**) Image of an immunostained section from the macaque monkey neocortex using an antibody to α-SMA and showing Alexa Fluor 633 labeling. (**l**) Image of an immunostained section of mouse neocortex with an antibody to GLUT1 and showing Alexa Fluor 633 labeling. (**m**) Image of a mouse aorta labeled with Alexa Fluor 633 and collected by using 2 mW two-photon laser power. (**n**) Image of a mouse femoral artery stained with an antibody to laminin and showing Alexa Fluor 633 labeling. *In vivo* images (**a**–**f**) were not background-subtracted or movement-corrected.

NIH-PA Author Manuscript

NIH-PA Author Manuscript

NIH-PA Author Manuscript

Images shown in **k**, **l** and **n** were collected with sequential scanning confocal microscopy. Scale bars, 100 μm (**a**–**g**), 10 μm (**k**,**l**,**n**) and 50 μm (**m**).

NIH-PA Author Manuscript
NIH-PA Author Manuscript
NIH-PA Author Manuscript

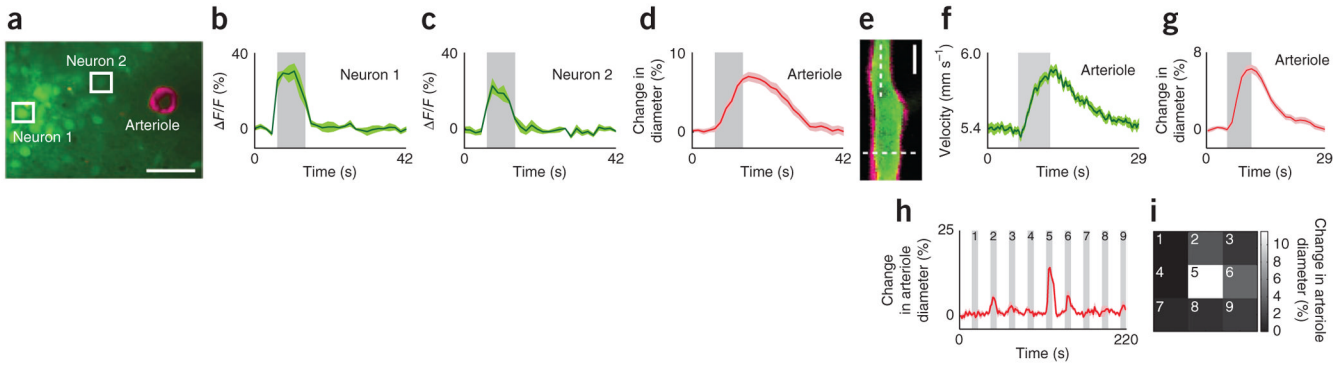

Figure 2.

Monitoring sensory stimulus–evoked responses in arterioles and adjacent neurons. (**a**–**d**) Simultaneous tracking of neuronal activation using the calcium dye Oregon Green 488 Bapta-1 acetoxymethyl ester (OGB-1 AM) and changes in arteriole diameter using Alexa Fluor 633 in layer 2/3 of the cat visual cortex. Image of an Alexa Fluor 633–labeled (magenta) penetrating arteriole and adjacent neuronal cell bodies labeled with OGB-1 AM (green) (**a**). Scale bar, 50 μm. Time courses (averages of 24 trials) of responses to drifting grating visual stimuli from neurons (**b**,**c**) and arteriole (**d**) marked in **a**. Δ*F*/*F*, relative change in fluorescence. (**e**–**g**) Measurement of red blood cell velocity and vessel diameter in an arteriole of the rat visual cortex. Imaged field of view (**e**) showing an arteriole labeled with Alexa Fluor 633 (magenta) and its lumen labeled with fluorescein dextran (green). Scale bar, 20 μm. Time courses (averages of 32 trials) of increases in velocity (**f**) and diameter (**g**) in response to drifting grating visual stimuli measured at locations marked by dotted lines in **e**. (**h**,**i**) Dilation of an Alexa Fluor 633–labeled arteriole in the cat visual cortex (**h**) in response to the presentation of visual stimuli in each of the nine locations (3 × 3 grid) of a stimulus display monitor (**i**). Average responses to five repeats of the entire visual stimulus sequence are plotted in **h**. The response to each stimulus position is plotted in the corresponding location in the 3 × 3 grid in which the luminance value represents the dilation magnitude. All gray bars, period of visual stimulation; error bands, s.e.m.

NIH-PA Author Manuscript

NIH-PA Author Manuscript

NIH-PA Author Manuscript

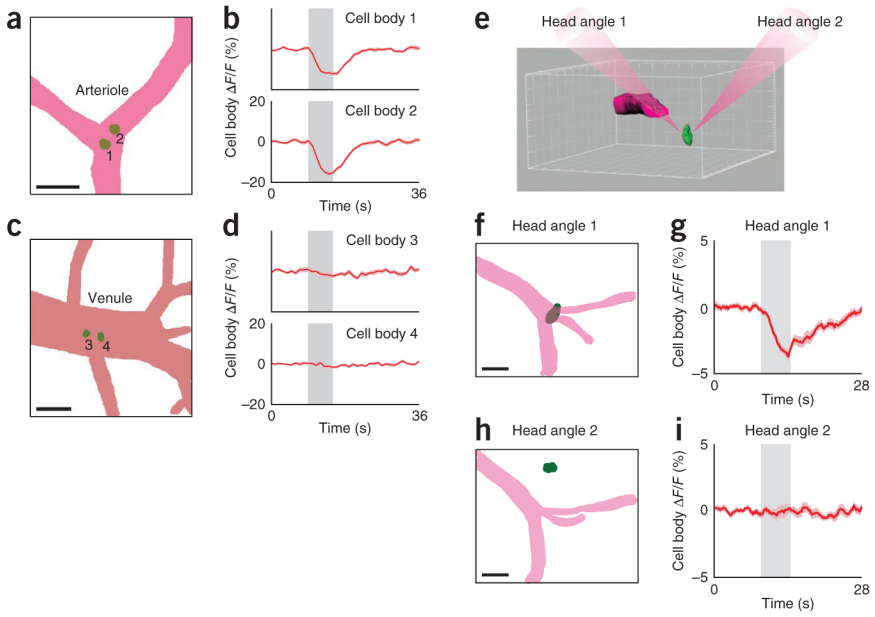

Figure 3.

Stimulus-dependent modulation of fluorescence in neurons located under cortical surface arterioles but not venules. (**a**–**d**) Mask representations of the dorsal view of a surface arteriole (**a**), venule (**c**) and underlying neuronal soma (labeled 1–4) in the rat visual cortex, and Alexa Fluor 594 fluorescence in the indicated neurons after a visual stimulus, in the same rat (**b**,**d**; averages of 23 trials). (**e**) Rendering of a surface arteriole (magenta) and a neuronal soma (green) in an imaged cortical volume, illustrating the potential dependence of the neuronal imaging artifact on the relative positioning of an arteriole and a nearby neuron. The two paths of light were achieved by rotating the head of a mouse that was positioned under the two-photon microscope's objective lens. In head angle 1, light passes through the surface arteriole. In head angle 2, light beam bypasses the arteriole. (**f**) Mask representation of an imaged area in mouse visual cortex (dorsal view) showing a surface arteriole (magenta) and a neuronal soma located directly below. (**g**) Alexa Fluor 594 fluorescence from the soma shown in **f** in response to visual stimuli. (**h**) Dorsal view of the same area as in **f** but after head rotation; soma is no longer under the arteriole. (**i**) Alexa Fluor 594 fluorescence in the soma shown in **h** in response to visual stimuli. Time courses in **g** and **i** are averages of 31 trials. All gray bars represent the period of visual stimulation; error bands, s.e.m.; scale bars, 50 μm.